Chinese Chemical Letters 36 (2025) 110335

Contents lists available at ScienceDirect

Chinese Chemical Letters

journal homepage: www.elsevier.com/locate/cclet

ROS-responsive micelles co-loaded dexamethasone and pristimerin to restore the homeostasis of the inflammatory microenvironment for rheumatoid arthritis therapy

Ruifeng Liang[a,1], Yanbei Tu[a,1], Peng Hua[a], Yongzhuo Huang[b], Meiwan Chen[a,*]

[a] State Key Laboratory of Quality Research in Chinese Medicine, Institute of Chinese Medical Sciences, University of Macau, Macau SAR 999078, China
[b] Zhongshan Institute for Drug Discovery, Shanghai Institute of Materia Medica, Chinese Academy of Sciences, Zhongshan 528437, China

ARTICLE INFO

Article history:
Received 27 February 2024
Revised 7 August 2024
Accepted 11 August 2024
Available online 12 August 2024

Keywords:
Rheumatoid arthritis
Micelles
Macrophages
Fibroblast-like synoviocytes
Osteoclastogenesis

ABSTRACT

Invasive fibroblast-like synoviocytes (FLS), inflammatory macrophages and osteoclasts are the main three contributors to rheumatoid arthritis (RA) progression by promoting synovial inflammation and destructing cartilage and bone. Targeting these three cell types for restoring the inflammatory homeostasis microenvironment may be a promising anti-RA strategy. Herein, we prepared a reactive oxygen species (ROS)-responsive micelles (DPTM) to co-load dexamethasone (DEX) and pristimerin (PRI) for RA therapy. This ROS-responsive system exhibits the following advantages: (1) It makes use of the "ELVIS" effect for passive delivery and targeting the ROS environment of RA-related cells to rapidly release the payload drugs DEX and PRI. (2) Compared with free drugs, DPTM showed stronger effect on the inhibition of RA-FLS proliferation and the promotion of RA-FLS apoptosis. Moreover, DPTM could significantly weaken the migration ability of RA-FLS as indicated by the results of wound healing assay and transwell assay. (3) DPTM exerted stronger cellular uptake and anti-inflammatory effect in M1 macrophages. (4) In the model studying receptor activator of nuclear factor kappa-B ligand (RANKL)-induced differentiation of bone marrow-derived macrophages (BMDMs) to osteoclasts, DPTM showed a stronger inhibitory activity on osteoclast formation as compared to free drugs. Taken together, these results highlighted the potential of DPTM for targeted RA therapy *via* inhibition of RA-FLS abnormal activation, macrophage polarization and osteoclastogenesis.

Rheumatoid arthritis (RA) is a classical chronic auto-immune disease, characterized by progressive synovial inflammation and the destruction of cartilage and bone, leading to joint deformities and ultimately limb disabilities [1,2]. Currently, a variety of medications are used to treat RA in clinics, including non-steroidal anti-inflammatory drugs (NSAIDs), glucocorticoids (GCs), disease-modifying anti-rheumatic drugs (DMARDs), and biologics. Although these drugs can relieve the symptoms and retard the progression of RA, they come with inherent drawbacks such as adverse side effects and low response rate over prolonged use [3,4]. Consequently, the development of new therapeutic strategies tailored to the inflammatory microenvironment of RA is critically necessary.

The pathological changes of RA involve the interaction of three cell types including inflammatory macrophages, invasive fibroblast-like synoviocytes (FLS), and osteoclasts [5-8]. They play significant roles in promoting the persistence of synovial inflammation and the destruction of cartilage and bone, which are considered as the key contributors within the RA microenvironment. To elaborate further, M1 macrophages aggravate the pathogenesis by releasing numerous classic inflammatory cytokines such as interleukin (IL)-1β, IL-6, and tumor necrosis factor (TNF)-α. These cytokines conversely promote inflammation by recruiting additional immune cells and triggering the activation of fibroblasts [9]. Concurrently, activated FLS exhibit tumor-like characteristics such as proliferation, migration, and invasion throughout the progression of RA, which in turn stimulate synovial vascularization, secrete a large amount of pro-inflammatory mediators, and promote the inflammatory process in RA-afflicted joints [10]. Furthermore, multi-nucleated osteoclasts possess the ability to specifically destroy mineralized cartilage and subchondral bone. Consequently, osteoclast-mediated bone resorption emerges as the primary contributor to bone erosion during RA progression [11]. Given these intricate interactions, targeting these three cell types to restore the homeostasis of the inflammatory microenvironment is a promising anti-RA strategy.

* Corresponding author.
E-mail address: mwchen@um.edu.mo (M. Chen).
[1] These authors contributed equally to this work.

https://doi.org/10.1016/j.cclet.2024.110335
1001-8417/

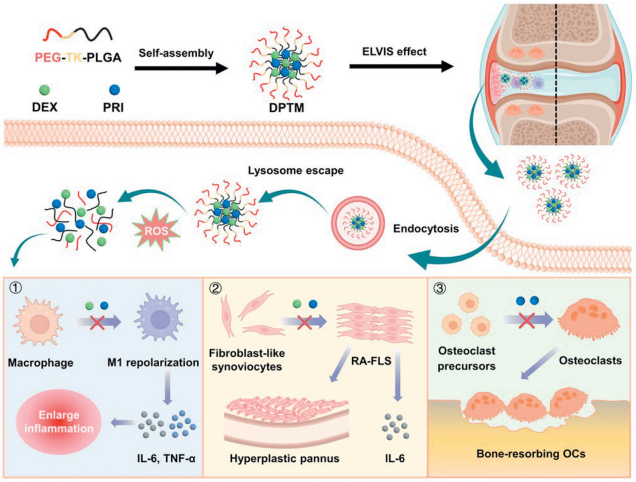

Scheme 1. Preparation process of DPTM and procedure for the treatment of RA. DPTM is passively targeted to the RA microenvironment through the ELVIS effect. Upon uptake of DPTM by microenvironment-associated cells (M1 macrophages, RA-FLS, osteoclasts), lysosomal escape of DPTM and cleavage of DPTM by endogenous ROS promoted the release of DEX and PRI. DPTM remodeled the homeostasis of the RA inflammatory microenvironment by inhibiting M1 macrophage activation, RA-FLS abnormal activation, and osteoclast formation.

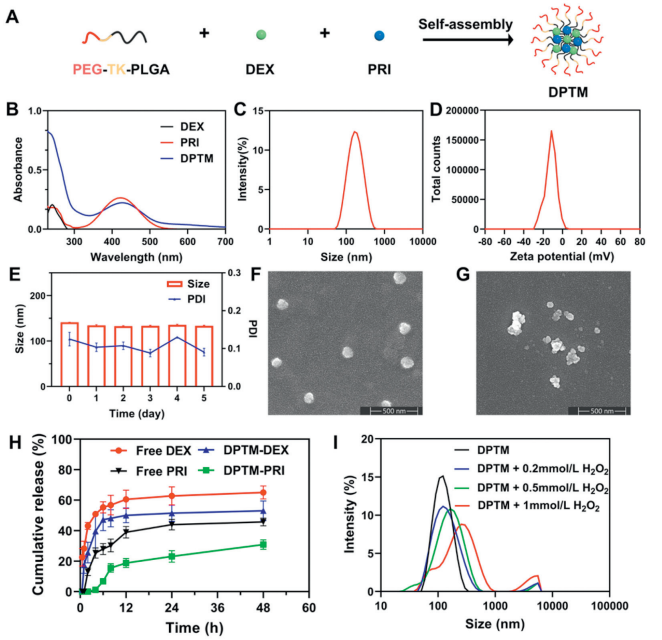

Fig. 1. Characterization of DPTM. (A) Schematic diagram of the preparation of DPTM. (B) UV spectrum of DPTM. (C) Particle size and (D) zeta potential of DPTM determined by DLS ($n = 3$). (E) Stability test of the DPTM in PBS at 37 °C ($n = 3$). (F, G) SEM images of DPTM and DPTM added 10 mmol/L H_2O_2. Scale bar: 500 nm. (H) *In vitro* release profiles of the DEX and PRI formulations ($n = 3$). (I) Particle size changes of DPTM in response to various ROS conditions. Data are presented as mean ± standard deviation (SD).

Pristimerin (PRI), a naturally occurring quinone methide triterpene, possesses various pharmacological properties such as anti-inflammatory, anti-peroxidative and anti-cell migration effects [12]. PRI has been reported to exert potential anti-arthritic effects in human RA-FLS, as well as prevent cartilage and bone damage in RA joints by modulating the expression of receptor activator of nuclear factor kappa-B ligand (RANKL) and pro-inflammatory cytokines, thereby disrupting the detrimental cell interactions that drive RA progression [13,14]. On the other hand, dexamethasone (DEX), a commonly used glucocorticoid for RA treatment, exerts its therapeutic influence by inhibiting the transcription of nuclear factor kappa-B (NF-κB), which interferes with the accumulation of macrophages and thus reduces the massive production of pro-inflammatory cytokines and chemokines [15,16]. DEX also converts M1-type macrophages into M2-type macrophages, which is beneficial to alleviate the inflammatory process [17].

Nano-drug delivery systems exhibit improved passive accumulation at the RA sites due to the "ELVIS" effect (extravasation through leaky vasculature and subsequent inflammatory cell-mediated sequestration), which resulted in enhanced drug accumulation and reduced side effects [18]. In addition, RA synovial joints contain higher levels of reactive oxygen species (ROS) compared to other tissues. Excessive ROS promotes the secretion of inflammatory cytokines, and continuous oxidative stress leads to bone and cartilage destruction, thereby accelerating the progression of RA [19,20]. Consequently, employing ROS-responsive materials as carriers for targeted drug delivery to RA joints serves a dual purpose: It can not only alleviate ROS-induced damage to RA cartilage but also facilitate drug release in inflammatory joints. Therefore, the combination of the ELVIS effects as well as ROS-responsive nanoparticles with enhanced drug target selectivity is a promising delivery strategy for RA treatment.

In this study, we fabricated ROS-responsive micelles (DPTM) to co-load DEX and PRI for RA therapy (Scheme 1). This system was formulated using thioketal (TK)-conjugated poly(lactic-*co*-glycolic acid)-polyethylene glycol *block* co-polymer ($PLGA_{10k}$-TK-PEG_{2k}) by solvent evaporation method, which could undergo rapid degradation in the presence of ROS in inflammatory tissues to release DEX and PRI due to the cleavage of TK bond. Additionally, DPTM showed significant anti-inflammatory effect on M1 macrophages and RA-FLS. Furthermore, it demonstrated stronger effects on the inhibition of proliferation, the promotion of apoptosis, and the inhibition of migration compared to free DEX and PRI in RA-FLS. In an osteoclast model, DPTM showed an obvious inhibitory activity against osteoclast formation. In conclusion, this work provides a feasible solution for the clinical treatment of RA by disrupting the complex cell interactions contributing to RA progression.

First, ROS-responsive polymer $PLGA_{10k}$-TK-PEG_{2k} was self-assembled with DEX and PRI by co-solvent evaporation to obtain DPTM for the treatment of RA (Fig. 1A). The ROS-responsiveness of the TK bonds of polymer had been verified using ^1H nuclear magnetic resonance spectroscopy (NMR) as shown in Fig. S1 (Supporting information). After incubating $PLGA_{10k}$-TK-PEG_{2k} with different concentrations of H_2O_2, the intensity of the sulfhydryl characteristic peak of the cleavage product, 3-mercaptopropionic acid, enhanced in a H_2O_2 concentration-dependent manner. The ultraviolet (UV) spectrum showed that DPTM contained the characteristic absorption peaks of PRI with a slight redshift (Fig. 1B). In the infrared spectrum, the significant peaks of the stretching vibration of C=O in α,β-unsaturated ketones and the bending vibration of the benzene ring were detected at 1663 cm^{-1} in DEX and 1448 cm^{-1} in PRI (Fig. S2 in Supporting information), identifying the presence of DEX and PRI in DPTM. Average particle size of DPTM was 141.1 ± 0.3 nm, PDI was 0.125 ± 0.018, and zeta potential was −11.93 ± 0.45 mV (Figs. 1C and D), which were measured by dynamic light scattering (DLS). The scanning electron microscope (SEM) image in Fig. 1F illustrated that the morphology of DPTM was spherical-like and uniformly distributed, which was consistent with the results obtained by DLS. Following expectations, the DPTM by adding H_2O_2 showed aggregation and drastic particle size changes, and the morphology changed from a round-like to an irregular shape (Fig. 1G). The micelle stability experiments pointed out that the micelles maintained a good particle size distribution over a period of 5 days at 37 °C and maintained a stable particle size at 10% fetal

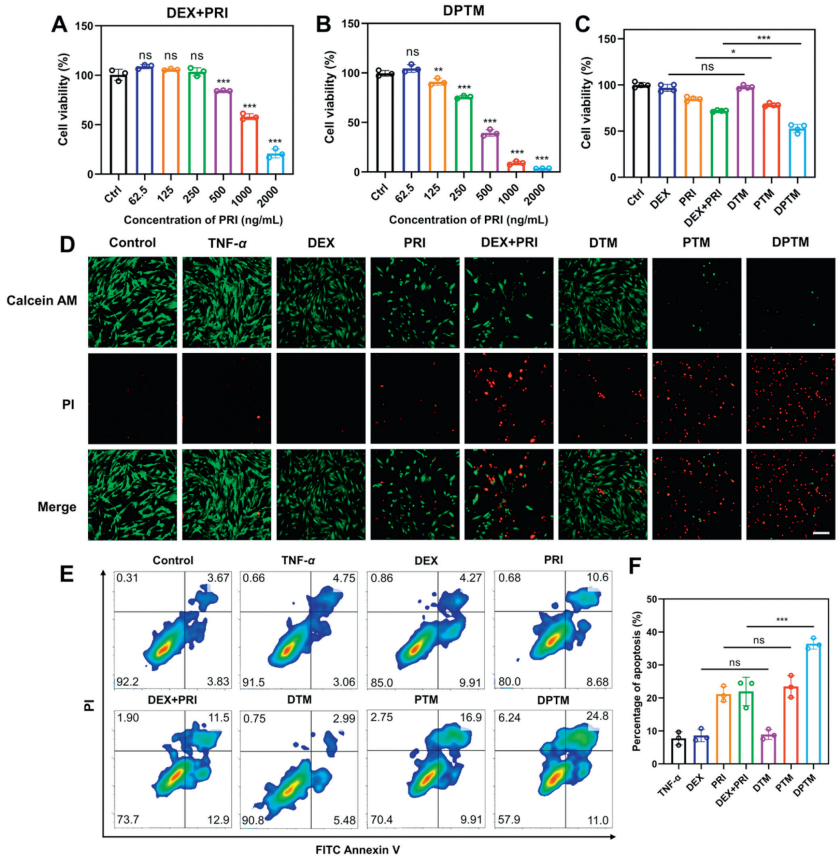

Fig. 2. Effect of DPTM on RA-FLS proliferation and apoptosis. (A, B) Cell viability determination after treatment with DEX+PRI and DPTM in RA-FLS ($n = 3$). (C) Cell viability of RA-FLS after treatment with different drugs at a concentration of 500 ng/mL ($n = 4$). (D) Live-dead staining of MH7A cells after treatment with different drugs at an equivalent concentration (500 ng/mL of PRI). Scale bar: 200 μm. (E) The flow cytograms of apoptosis experiments after treatments at a PRI concentration of 250 ng/mL. (F) Quantitative analysis of the apoptosis experiments after treatments. Data are presented as mean ± SD. The statistical significance of the data was assessed using Student's *t*-test or one-way analysis of variance (ANOVA). ns, not significant. $^{*}P < 0.05$, $^{**}P < 0.01$, $^{***}P < 0.001$.

bovine serum (FBS) at 37 °C for 48 h (Fig. 1E and Fig. S3 in Supporting information). In addition, DPTM was found to possess a good encapsulation efficiency (EE%), which were 60.4% ± 5.7% and 93.3% ± 4.5% for DEX and PRI, respectively. Drug loading capacity of DPTM were 5.1% ± 0.5% for DEX and 2.8% ± 0.1% for PRI. These properties of DPTM allowed it to be passively targeted to the inflammatory microenvironment for drug release *via* the ELVIS effect. *In vitro* release experiments, the release of DEX and PRI in DPTM was remarkably less than that of free DEX and PRI. After 4 h of release, the release rates of free DEX and PRI were 50.9% ± 1.1% and 25.4% ± 2.8%, and the release degrees of the two drugs in DPTM were only 39.7% ± 9% and 1.2% ± 0.7%, respectively. After 48 h, the release rates of free DEX and PRI increased to 65.1% ± 3.5% and 45.7% ± 2%, while the counterparts of DPTM were only 53% ± 5.2% and 30.9% ± 2.6%, suggesting that DPTM decelerated the release of the drugs, which was expected to improve the anti-RA efficacy of the drugs (Fig. 1H). To examine the release of DPTM under ROS environment, DPTM was co-incubated with different concentrations of H_2O_2, and the results showed that DPTM underwent a more pronounced change in particle size with increasing concentration of H_2O_2, indicating that DPTM was cleaved and the drugs were released (Fig. 1I).

To verify whether polymer $PLGA_{10k}$-TK-PEG_{2k} as a carrier could improve the efficiency of intracellular uptake, we used coumarin (C6) as a dye to replace the drug in DPTM. CTM is a micellar preparation formed by self-assembly of C6 and $PLGA_{10k}$-TK-PEG_{2k} to display the state of cell uptake. The drug uptake was tested in TNF-α activated MH7A cells which mimic the properties of RA-FLS, and the results showed a time-dependent drug uptake in RA-FLS. As depicted in Figs. S4A and C (Supporting information), intracellular C6 fluorescence was enhanced in the CTM-treated group than that of the drug-free group from 0.5 h to 2 h. Quantification of C6 in RA-FLS using flow cytometry (Figs. S4B and D in Supporting information) showed that the relative uptake efficiency of the free C6 group was 50.3% after 2 h of uptake by RA-FLS, whereas that of CTM reached 97.1%. The fluorescence intensity of CTM in RA-FLS was consistently higher compared to that of free C6 at all periods (Fig. S5 in Supporting information), suggesting that nano-micelles could dramatically improve the cellular uptake efficiency of RA-FLS. The high cellular uptake of CTM could be attributed to the good biocompatibility of the micellar formulations.

RA-FLS are a critical part of the invasive synovium that leads to RA, which constantly triggers destructive joint inflammation, stemming from its ability to modulate immuno-inflammation, eventually resulting in joint and cartilage damage. In addition, RA-FLS exhibit distinctive invasiveness, which enhances inflammatory damage [21,22]. Therefore, targeting the inflammatory activation and invasive properties of RA-FLS using nanoparticles serves as a strategy for the treatment of RA. Anti-proliferative and anti-invasive effects of PRI monotherapies on RA-FLS have been employed in the literature to slow down the development of RA [23]. Hence, we had investigated the effect of DPTM on RA-FLS proliferation using MTT assay, the cell viability of RA-FLS was dose-dependently decreased in the free DEX + PRI group (Fig. 2A) and DPTM group (Fig. 2B). However, it was noted that DPTM exhibited higher cytotoxicity than the free drug group at all corresponding concentra-

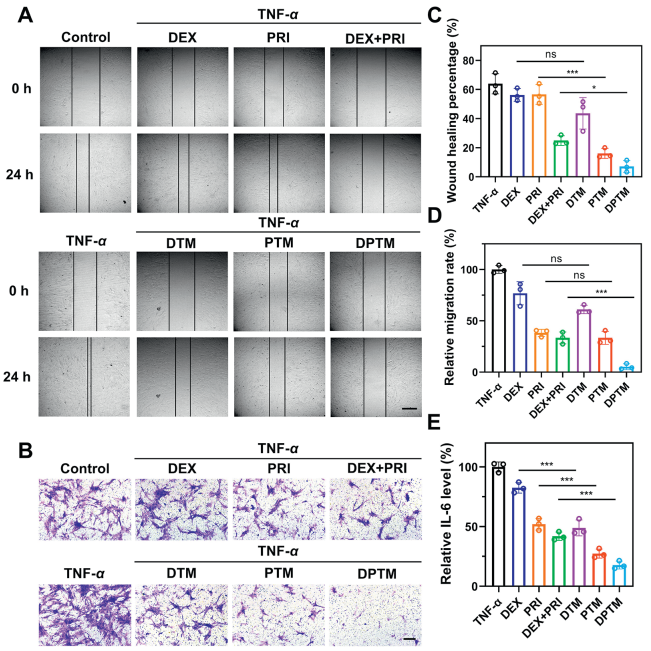

Fig. 3. Effect of DPTM on RA-FLS migration and cytokine production. (A) Representative pictures of wound healing assay in RA-FLS, black lines indicate the cell-free areas. (B) Representative pictures of the transwell migration assay in RA-FLS. (C) Quantitative analysis of the width in the wound healing assay after various drug treatments ($n = 3$). (D) Quantitative analysis of the relative migration rate in the transwell migration assay after treatment ($n = 3$). (E) Relative IL-6 levels determined by ELISA in RA-FLS culture supernatants after treatment of different drug or micellar formulations. Scale bar: 500 μm. Data are presented as mean ± SD. The statistical significance was assessed using one-way ANOVA. $^{*}P < 0.05$, $^{***}P < 0.001$.

tions in RA-FLS. At a PRI concentration of only 500 ng/mL, DPTM could kill more than 50% of the cells, whereas the combination of free DEX and PRI could only kill about 30% (Fig. 2C). The live-dead staining assay (Fig. 2D) showed DEX and DTM did not inhibit RA-FLS proliferation. In contrast, the micelles groups exhibited more dead cells than the free PRI. In particular, severe cell mortality was noted in the PTM and DPTM groups. The enhanced cytotoxicity of DPTM against RA-FLS could be attributed to the higher cellular uptake and specific release induced by the PEG modification and ROS-responsive properties on the DPTM surface.

Subsequently, we detected whether these micellar formulations could affect the apoptosis of RA-FLS. Since DPTM had significant anti-proliferative activity at a PRI concentration of 250 ng/mL, the effect of DPTM on RA-FLS apoptosis was further explored at this concentration. Flow cytometry analysis showed that DPTM exhibited the strongest apoptosis rate in TNF-α-stimulated MH7A cells compared with free PRI and DEX + PRI (Fig. 2E). The apoptosis rate was obtained by summing early apoptosis and late apoptosis. Although there was no statistical difference, DEX + PRI induced relatively more late apoptosis than PRI. Quantitative analysis of the apoptosis rate showed a statistically significant difference in apoptosis rate between the DPTM and the free DEX + PRI group, indicating that the apoptosis rate of free drugs was increased after being prepared into micelles (Fig. 2F).

The ability of DPTM to inhibit RA-FLS migration had been demonstrated using wound healing assays and transwell migration assay with TNF-α-stimulated MH7A cells. The DEX and PRI concentrations were 200 and 100 ng/mL in the wound healing assay and transwell migration assay, respectively, which had almost no toxicity to RA-FLS. As shown in Fig. 3A, TNF-α stimulation significantly promoted the migration of MH7A cells after 24 h incubation, but this trend was significantly attenuated by free DEX+PRI and micellar formulations. Quantitative analysis of wound healing results showed that the percentage of wound healing was below 25% for DEX + PRI, PTM and DPTM (Fig. 3C). These observations were consistent with published results [23,24]. Furthermore, a transwell migration assay was also performed to validate the anti-migratory effect, and the results showed that the micellar formulations corresponding to the free drug had stronger anti-migration ability, especially DPTM, which had less than 10% cell migration (Figs. 3B and D). Enzyme linked immunosorbent analysis (ELISA) of representative inflammatory factor IL-6 in RA-FLS demonstrated that the anti-inflammatory effects of free DEX and PRI were weaker than the combination group. Furthermore, a transwell migration assay was also performed to validate the anti-migratory effect, and the results showed that the micellar formulations corresponding to the free drug had stronger anti-migration ability, especially DPTM, which had less than 10% cell migration (Figs. 3B and D). ELISA analysis of representative inflammatory factor IL-6 in RA-FLS demonstrated that the anti-inflammatory effects of free DEX and PRI were weaker than the combination group of two drugs, and the inhibitory effect of micellar formulations on IL-6 was generally greater than the corresponding free drug, with DPTM having the most potent anti-inflammatory effect (Fig. 3E).

Macrophages are highly plastic and systemic cells. When it is activated to the M1 phenotype in RA, macrophages may rapidly change in morphology and protein expression, and migrate to inflammatory sites [9]. Pro-inflammatory M1 macrophages drive the progression of RA by secreting a variety of cytokines (*e.g.*, TNF-α, IL-1β, IL-6) and chemokines, making them promising therapeutic targets in strategies to treat arthritic inflammation [25].

Therefore, we investigated the uptake efficiency of M1 macrophages to the constructed nano-micelles in lipopolysaccharide (LPS)-activated macrophages which exhibited the characteristics of M1 macrophages. We found that intracellular uptake of CTM by both undifferentiated macrophages (Figs. S6A and C in Supporting information) and M1 macrophages (Figs. S6B and D in Supporting information) was significantly higher than that of free C6 at all 4-time points, suggesting that the construction of nano-micelles could significantly enhance the intracellular uptake efficiency of the drug. Interestingly, by comparing the mean fluorescence intensity (MFI) ratio of C6 and CTM in macrophages and M1 macrophages, we found that the MFI ratio of CTM and C6 in macrophages was lower than in M1 macrophages within 2 h, indicating that the nano-micelles were taken up more by M1 macrophages (Fig. S6E in Supporting information).

To further investigate the fate of CTM in inflammatory macrophages, co-localization experiments were carried out in M1 macrophages. After 2 h of incubation, the green fluorescence of CTM showed good co-localization with lysosomes stained red by Lysotracker, confirming the internalization of nano-micelles. After 12 h of incubation, the green fluorescence of C6 was significantly enhanced and was mainly concentrated in the cytoplasm, pointing to the escape of more CTM from the lysosomes. Quantitative data were determined by the Pearson correlation coefficient (PCC), the PCC of C6 and Lysotracker Red decreased from 0.46 to 0.08 after 2 h and 12 h of uptake, proving that a large number of nano-micelles escaped from the lysosome after 12 h of uptake (Fig. S7 in Supporting information).

To prevent efficacy experiments from being influenced by drug cytotoxicity, cytotoxicity assays were performed on M1 macrophages and osteoclasts as shown in Fig. S8 (Supporting information). The concentrations used in subsequent cellular experiments were within the range of no cytotoxicity. For exploring the anti-inflammatory effect of DPTM in activated macrophages, the expression of M1 macrophage marker CD86 and M2 macrophage marker CD206 were first determined by flow cytometry in LPS-induced RAW264.7 cells. The results showed that the M1 polarization could be inhibited by free drugs and corresponding micel-

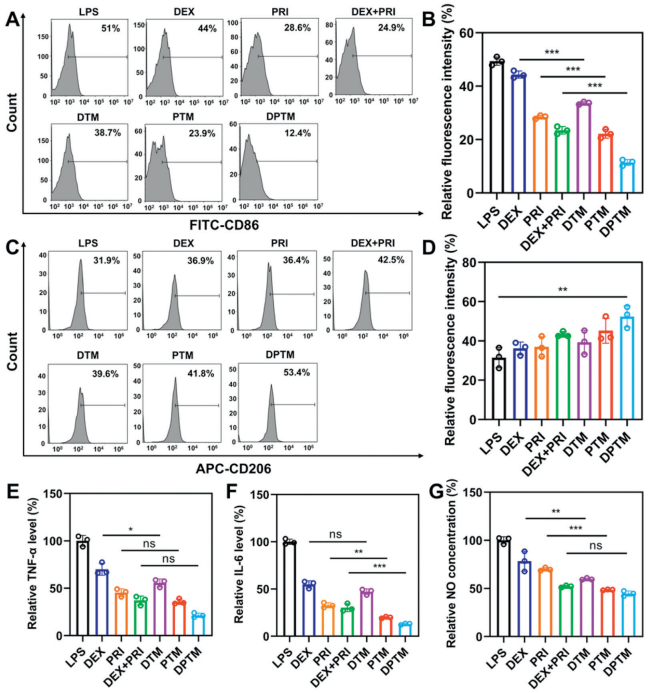

Fig. 4. Anti-inflammatory effect of DPTM in M1 macrophages. RAW264.7 cells were pretreated with free drugs or formulations for 4 h, and then were stimulated with LPS for 6 h, followed by quantitative analysis of (A) FITC-CD86 and (C) APC-CD206 using flow cytometry. (B) Relative FITC fluorescence intensity and (D) relative APC fluorescence intensity in different treatment groups. M1 macrophages were treated with free drugs and micellar formulations for 24 h, and then (E) relative TNF-α and (F) IL-6 levels were measured by ELISA kits. (G) NO levels in M1 macrophage supernatant after treatment of different drug or micellar formulations. Data are presented as mean ± SD. The statistical significance was assessed using one-way ANOVA. $^{*}P < 0.05$, $^{**}P < 0.01$, $^{***}P < 0.001$.

lar formulations. In particular, the strongest inhibition of CD86 expression was exhibited by DPTM, which dropped from 49.4% ± 1.3% to 11.4% ± 0.9% (Figs. 4A and B), suggesting that the micelles were able to inhibit M1 polarization and thus exerted anti-inflammatory effects. Furthermore, activated macrophages treated with DPTM had the most APC-CD206 fluorescence intensity, indicating that DPTM promoted the polarization of M1 macrophages to M2 macrophages (Figs. 4C and D). Consistently, the determination of cytokine levels revealed that both the free drugs and the corresponding micellar formulations could significantly decrease TNF-α and IL-6 levels in M1 macrophages, and again highlighted the excellent anti-inflammatory effects of DPTM (Figs. 4E and F). Proteolytic degradation of inducible nitric oxide synthase (iNOS) is one of the key mechanisms by which DEX regulates the production of nitric oxide (NO) in stimulated RAW 264.7 cells [26,27]. Similar to DEX, PRI down-regulated NO production by inhibiting the expression of iNOS [28]. Both DEX and PRI preparations reduced NO levels in the supernatant of M1 macrophages, and the micellar group exhibited a stronger inhibition of NO, suggesting that micelles could effectively exert an anti-inflammatory effect (Fig. 4G). Inhibition of pro-inflammatory levels in M1 macrophages and RA-FLS directly inhibited migration and proliferation of inflammatory cells, thereby restoring the homeostasis of the RA microenvironment, consistent with results reported in the literature [29-31].

Patients with RA are often associated with severe local and systemic bone loss, which is frequently due to increased osteoclast-mediated bone resorption. Osteoclast differentiation is influenced by a variety of factors and is closely associated with inflammatory cell activation during RA progression, including macrophages and RA-FLS, which accelerates bone destruction. Inhibition of osteoclastogenesis and bone erosion has been accepted as an effective strategy for the long-term preservation of joint architecture in RA patients while treating RA [32,33]. Therefore, the ability of DPTM on osteoclast differentiation was determined in the RANKL-induced osteoclastogenesis model. Administration doses of PRI on the inhibition of osteoclastogenesis vary widely in the literature [13,14,34], thus the appropriate concentration to investigate the effect of PRI on osteoclastogenesis needs to be screened. Since bone marrow-derived macrophages (BMDMs) did not display cellular damage at PRI concentrations of 12.5 and 25 ng/mL (Fig. S9 in Supporting information), the equivalent PRI concentration of 25 ng/mL was selected for testing the effect of the drugs on osteoclast differentiation. As shown in Fig. 5A, tartrate resistant acid phosphatase (TRAP) staining was used to visualize mature osteoclasts. RANKL stimulation for 7 days significantly induced the differentiation of the osteoclast precursor BMDMs to the mature osteoclasts. PRI-containing formulations could inhibit osteoclastogenesis and DPTM showed the strongest inhibitory activity, as indicated by the reduc-

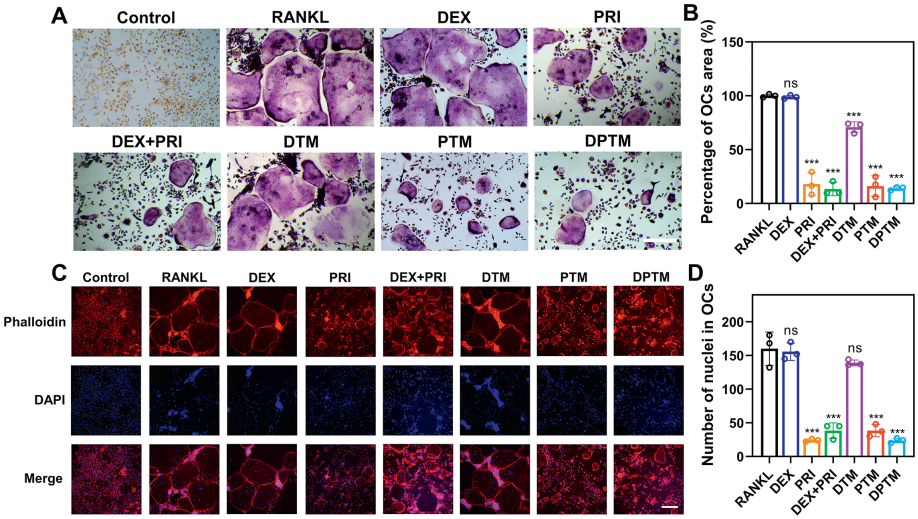

Fig. 5. Effect of DPTM on RANKL-induced osteoclastogenesis *in vitro*. Representative (A) TRAP staining and (C) F-acting ring staining of osteoclasts after treatment with different drugs and micellar formulations. Scale bar: 200 μm. (B) Quantitative analysis of osteoclast area of different groups in TRAP staining ($n = 3$). (D) Quantitative analysis of nuclei number in osteoclasts in F-acting ring staining ($n = 3$). Data are presented as mean ± SD. The statistical significance was assessed using Student's *t*-test. $^{***}P < 0.001$ *vs.* the RANKL treated group.

tion in the area of TRAP-positive multinucleated osteoclasts (Fig. 5B). However, this effect was not found for DEX. The F-actin ring is a unique cytoskeletal structure of mature osteoclasts and is essential for osteoclasts to perform bone resorption functions. Phalloidin staining revealed that RANKL stimulation resulted in the formation of F-actin rings of osteoclasts, but these F-actin rings were inhibited by treatment of PRI-containing formulations instead of DEX formulations, which was consistent with TRAP staining results (Fig. 5C). Analysis of Fig. 5D indicated that the number of nuclei in F-actin rings is remarkably decreased under treatment with PRI-containing formulations. Collectively, the ability of DPTM to inhibit osteoclast formation enabled it to significantly reduce bone loss and protect joint structure when used in RA therapy.

In conclusion, we constructed a ROS-responsive nano-micelle DPTM coloaded with DEX and PRI to attenuate the progression of RA disease by remodeling the homeostasis of the RA inflammatory microenvironment. Due to its uniform particle size distribution, stability and PEG modification, DPTM significantly improved the passive targeting of RA pathological cells as well as drug uptake. DPTM is also ROS-responsive, which enables DPTM not only to eliminate endogenous ROS in inflammatory cells specifically, but also to respond to ROS cleavage for rapid release of therapeutic drugs DEX and PRI. DPTM significantly inhibited the proliferation and migration of RA-FLS, inhibited M1 polarization, and promoted M2 polarization, as well as inhibited the production of inflammatory cytokines in M1 macrophages, and inhibited the differentiation and maturation of osteoclasts, which can restore the pathological cellular balance in the RA microenvironment, and ultimately exert the anti-RA effect. This study provides an effective strategy for RA treatment through the regulation of "RA-FLS-macrophages-osteoclasts" to remodel the RA microenvironmental homeostasis.

Declaration of competing interest

The authors declare that they have no known competing financial interests or personal relationships that could have appeared to influence the work reported in this paper.

CRediT authorship contribution statement

Ruifeng Liang: Writing – original draft, Visualization, Methodology, Formal analysis. **Yanbei Tu:** Writing – review & editing, Visualization, Resources, Investigation, Data curation. **Peng Hua:** Visualization, Conceptualization. **Yongzhuo Huang:** Writing – review & editing, Resources. **Meiwan Chen:** Writing – review & editing, Supervision, Project administration, Funding acquisition.

Acknowledgments

This study was supported by the National Natural Science Foundation of China (No. 82204724), the Science and Technology Development Fund, Macau SAR (Nos. 0029/2023/AFJ, 005/2023/SKL), the Multi-Year Research Grant (MYRG) of University of Macau (Nos. MYRG2022-00203-ICMS, MYRG-GRG2023-00134-ICMS-UMDF) and Macao Young Scholars Program (No. AM2022019).

Supplementary materials

Supplementary material associated with this article can be found, in the online version, at doi:10.1016/j.cclet.2024.110335.

References

[1] Q. Ding, W. Hu, R. Wang, et al., Signal Transduct. Target. Ther. 8 (2023) 68.
[2] G. Simons, J. Caplan, R.L. DiSantostefano, et al., Arthritis Res. Ther. 24 (2022) 55.
[3] A.F. Radu, S.G. Bungau, Ageing Res. Rev. 87 (2023) 101927.
[4] A.F. Radu, S.G. Bungau, Cells 10 (2021) 2857.
[5] R.I. Ainsworth, D. Hammaker, G. Nygaard, et al., Nat. Commun. 13 (2022) 6221.
[6] M.A. Boutet, G. Courties, A. Nerviani, et al., Autoimmun. Rev. 20 (2021) 102758.
[7] K. Yokota, K. Sato, T. Miyazaki, et al., Arthritis Rheumatol. 73 (2021) 1145–1154.
[8] N. Komatsu, H. Takayanagi, Nat. Rev. Rheumatol. 18 (2022) 415–429.
[9] S. Tardito, G. Martinelli, S. Soldano, et al., Autoimmun. Rev. 18 (2019) 102397.
[10] Z. Wang, J. Wang, T. Lan, et al., Front. Immunol. 14 (2023) 1135384.
[11] Q. Niu, J. Gao, L. Wang, et al., Front. Immunol. 13 (2022) 1034050.
[12] V.M. Dirsch, A.K. Kiemer, H. Wagner, A.M. Vollmar, Eur. J. Pharmacol. 336 (1997) 211–217.
[13] D. Qi, H. Liu, X. Sun, et al., Front. Pharmacol. 11 (2020) 621110.
[14] X. Li, X. Lin, Z. Wu, et al., Drug Des. Dev. Ther. 15 (2021) 61–74.
[15] M. Lorscheider, N. Tsapis, M. Ur-Rehman, et al., J. Control. Release 296 (2019) 179–189.
[16] S. Sun, J. Zhang, H. Li, et al., J. Ethnopharmacol. 271 (2021) 113880.
[17] Y. Li, Q. Liang, L. Zhou, et al., Acta Biomater. 152 (2022) 406–424.
[18] F. Yuan, L. Quan, L. Cui, et al., Adv. Drug Deliv. Rev. 64 (2012) 1205–1219.
[19] A.R. Phull, B. Nasir, I.U. Haq, S.J. Kim, Chem. Biol. Interact. 281 (2018) 121–136.
[20] M.J. Smallwood, A. Nissim, A.R. Knight, et al., Free Radic. Biol. Med 125 (2018) 3–14.
[21] A.P. Croft, J. Campos, K. Jansen, et al., Nature 570 (2019) 246–251.
[22] N. Bottini, G.S. Firestein, Nat. Rev. Rheumatol. 9 (2013) 24–33.
[23] M. Lv, Q. Liang, Z. Luo, et al., Metabolites 12 (2022) 839.
[24] C.C. Yang, L.D. Hsiao, H.C. Tseng, et al., J. Inflamm. Res. 13 (2020) 325–341.
[25] Q. Wang, H. Jiang, Y. Li, et al., Biomaterials 122 (2017) 10–22.
[26] G. Walker, J. Pfeilschifter, U. Otten, D. Kunz, Biochim. Biophys. Acta Gen. Subj. 1568 (2001) 216–224.
[27] M. Söderberg, F. Raffalli-Mathieu, M.A. Lang, Mol. Immunol. 44 (2007) 3204–3210.
[28] H.J. Kim, G.M. Park, J.K. Kim, Arch. Pharmacal. Res. 36 (2013) 495–500.
[29] Y. Shen, L. Teng, Y. Qu, et al., J. Ethnopharmacol. 284 (2022) 114791.
[30] F. Liu, Y. Liu, S. Zhan, et al., Int. Immunopharmacol. 88 (2020) 106823.
[31] W. Jiao, J. Xu, D. Wu, et al., Phytomedicine 114 (2023) 154741.
[32] W. Sun, N. Meednu, A. Rosenberg, et al., Nat. Commun. 9 (2018) 5127.
[33] Y. Tu, L. Tan, T. Lu, et al., Biochem. Pharmacol. 197 (2022) 114912.
[34] Y. Wang, S. Chen, K. Du, et al., J. Ethnopharmacol. 279 (2021) 114368.